EMERGENCE OF AN INVARIANT REPRESENTATION OF TEXTURE IN PRIMATE SOMATOSENSORY CORTEX

Justin D. Lieber[1] and Sliman J. Bensmaia[1,2]

[1]Committee on Computational Neuroscience, University of Chicago, Chicago, IL

[2]Department of Organismal Biology and Anatomy, University of Chicago, Chicago, IL

ABSTRACT

A major function of sensory processing is to achieve neural representations of objects that are stable across changes in context and perspective. Small changes in exploratory behavior can lead to large changes in signals at the sensory periphery, thus resulting in ambiguous neural representations of objects. Overcoming this initial ambiguity is a hallmark of human object recognition across sensory modalities. Here, we investigate the perception of tactile texture, which is stable across a wide range of exploratory movements of the hand, including changes in scanning speed, despite the strong dependence of the peripheral response on hand movements. To probe the neural basis of speed-tolerant texture representations, we scanned a wide range of everyday textures across the fingertips of Rhesus macaques at multiple speeds and recorded the responses evoked in tactile nerve fibers and somatosensory cortical neurons (in Brodmann's areas 3b, 1, and 2). We found that, unlike afferents, individual cortical neurons exhibit a wide range of speed-sensitivities: some neurons are more strongly driven by changes in speed than peripheral afferents, while others exhibit responses that are nearly speed-independent. As a result, compared to the periphery, the cortical population exhibits 1) an increased ability to simultaneously encode independent representations of speed and texture, and 2) an increased ability to account for the speed-tolerant perception of texture in human subjects. Finally, we demonstrate that this separation of speed and texture information is a natural consequence of previously described cortical computations.

INTRODUCTION

We are endowed with a remarkable ability to identify objects across a wide range of contexts and perspectives. For example, we can visually identify objects in a fraction of a second, even over broad changes in lighting, distance, or viewing angle. Similarly, we can auditorily identify the timbre of voices and musical instruments across a wide range of loudness and pitches (Handel and Erickson, 2001; Marozeau et al., 2003). In both vision and audition, perceptual tolerance is achieved despite sensory representations at the periphery (the retina, the cochlea) that are highly dependent on perspective and context (Croner and Kaplan, 1995; Enroth-Cugell and Robson, 1966; Joris et al., 2011; Sachs and Young, 1979). Indeed, a signature of sensory processing is a progression of object representations that become increasingly robust to changes in context (Avidan et al., 2002; Cadieu et al., 2014; Finn et al., 2007; Metzen et al., 2016; Sadagopan and Wang, 2008; Walker et al., 2011).

In touch, the best known instance of perceptual tolerance is for texture: tactile texture perception has been shown to be nearly independent of the force exerted on the surface (Lederman, 1981; Lederman and Taylor, 1972) or the speed at which it is scanned across the skin (Boundy-Singer et al., 2017; Lederman, 1974; Meftah el-M et al., 2000). Remarkably, this perceptual tolerance is achieved despite responses in the somatosensory nerves that are strongly modulated by exploratory parameters such as scanning speed (DiCarlo and Johnson, 1999; Goodwin and Morley, 1987a; Phillips et al., 1992) and, to a lesser degree, force (Goodwin and Morley, 1987b; Phillips et al., 1992; Saal et al., 2017). The effect of scanning speed on texture coding in the nerve is particularly pronounced for fine textures, which are encoded in precisely timed, texture-specific spiking sequences that contract or dilate multiplicatively with increases and decreases in speed, respectively (Weber et al., 2013). Thus, to achieve a tolerant percept of texture, texture-specific information must be extracted from peripheral signals that are highly dependent on exploratory parameters.

As texture representations ascend the somatosensory neuraxis towards somatosensory cortex, precisely timed patterns of spatio-temporal activity are processed by canonical sensory transformations, such as differentiating filters that calculate spatial (Bensmaia et al., 2008; DiCarlo and Johnson, 2000; Sripati et al., 2006) and temporal (DiCarlo and Johnson, 2000; Saal et al., 2015; Sripati et al., 2006) variation across the peripheral signal. These filters extract perceptually-relevant stimulus information that may not be present in the firing rates of peripheral afferents (Connor 1990). It thus stands to reason that these same mechanisms could extract a speed-tolerant representation of texture that was not present in the peripheral response. Indeed, previous work suggests that a subpopulation of neurons in somatosensory cortex may exhibit speed-tolerant responses to texture (Bourgeon et al., 2016; Dépeault et al., 2013; DiCarlo and Johnson, 1999; Sinclair and Burton, 1991). However, these studies only characterized cortical responses to parametrically defined dot patterns and gratings that span a narrow range of tangible textures (Weber et al., 2013). Furthermore, these studies focused primarily on the speed-sensitivity of cortical neurons without comparing these effects to those seen in peripheral afferents.

In the present study, we seek to fill this gap by recording the responses of neurons in somatosensory cortex – including Brodmann's areas 3b, 1, and 2 – to natural textures scanned over the skin at various speeds, spanning the range used in natural texture exploration (Callier et al., 2015; Gamzu and Ahissar, 2001; Libouton et al., 2010; Morley et al., 1983; Tanaka et al., 2014). Using these data, we then directly compare how neuronal firing rate responses are modulated by speed in the nerve and in cortex. We find that while speed modulation is generally weaker in cortical firing rates than in afferent firing rates, this effect does not typically confer a more speed-tolerant texture code to individual cortical neurons. Rather, we find that speed-tolerant texture perception is best explained by an untangling of information about speed and texture across the responses of neuronal populations. The resulting cortical population response can better account for speed-tolerant texture perception than its peripheral counterpart.

RESULTS

We have previously reported the texture-evoked responses of 39 tactile afferents (Weber et al., 2013) and 141 neurons from somatosensory cortex (Lieber and Bensmaia, 2019), as many different textures were scanned over the skin. Here, we report the responses of a subset of those neurons to textures presented at different speeds. We recorded texture-evoked responses from 21 tactile fibers – 9 slowly adapting type 1 (SA1), 9 rapidly adapting (RA), and 3 Pacinian (PC) fibers — and 49 neurons in somatosensory cortex – 14 from area 3b, 26 from area 1, and 9 from area 2 – with receptive fields on the distal fingertip. For the peripheral nerve experiments, each of 55 different textures was scanned over the skin at 3 different speeds (40, 80, and 120 mm/s) using a rotating drum stimulator. For the cortical experiments, each of 10 different textures was scanned over the skin at 4 different speeds (60, 80, 100, and 120 mm/s), which spans the range of speeds spontaneously used to explore tactile textures (Callier et al., 2015; Gamzu and Ahissar, 2001; Libouton et al., 2010; Morley et al., 1983; Tanaka et al., 2014). We sought to determine the effect of scanning speed on the neural representation of texture, and how these representations change between periphery and cortex.

Speed-dependence of firing rates

We found that, for both tactile nerve fibers and cortical neurons, increasing the speed at which a texture is scanned across the skin drives an increase in the firing rate response (Figure *1A-C*). This effect was

significant for a majority of neurons at the periphery (20/21, p <0.05, permutation test) and in cortex (37/49). For consistency, we only included in the analysis the responses to textures that were either shared across the peripheral and cortical experiments or were similar (Supplementary Figure *1A*, see Methods). Using this matched set of textures, we compared the speed-sensitivity of peripheral afferents to that of cortical neurons by expressing sensitivity as a percentage increase in firing rate per doubling in speed (Supplementary Figure *1B-D*). Using this metric, we found that peripheral afferents exhibited more speed-sensitivity than did cortical neurons (Figure *1D*) (median across cells ± median absolute deviation (MAD), periphery: 28.7%±5.1%, cortex: 20.0%±11.5%, p<0.05 Wilcoxon rank-sum test, see also Supplementary Figure *1*E, result are consistent with previous experiments: Supplementary Table *1*). While we did observe significant differences in speed-sensitivity across different afferent classes (Delhaye et al., 2019), every submodality trended towards more speed-sensitivity than that was observed in cortex (RA: 29.3%±3.3% and PC: 35.0%±5.4%, p < 0.05, SA1: 23.8%±6.2%, p=0.18, see *Supplementary Figure 2A-B*). The speed-sensitivity of responses in area 3b trended towards smaller values than responses from areas 1 and 2 (area 3b: 12.9%±9.8% < area 1: 23.1%±7.5% at p<0.05 and area 2: 24.4%±24.9%, p=0.33, see Supplementary Figure 2A-B), consistent with previous reports (Bourgeon et al., 2016; Dépeault et al., 2013).

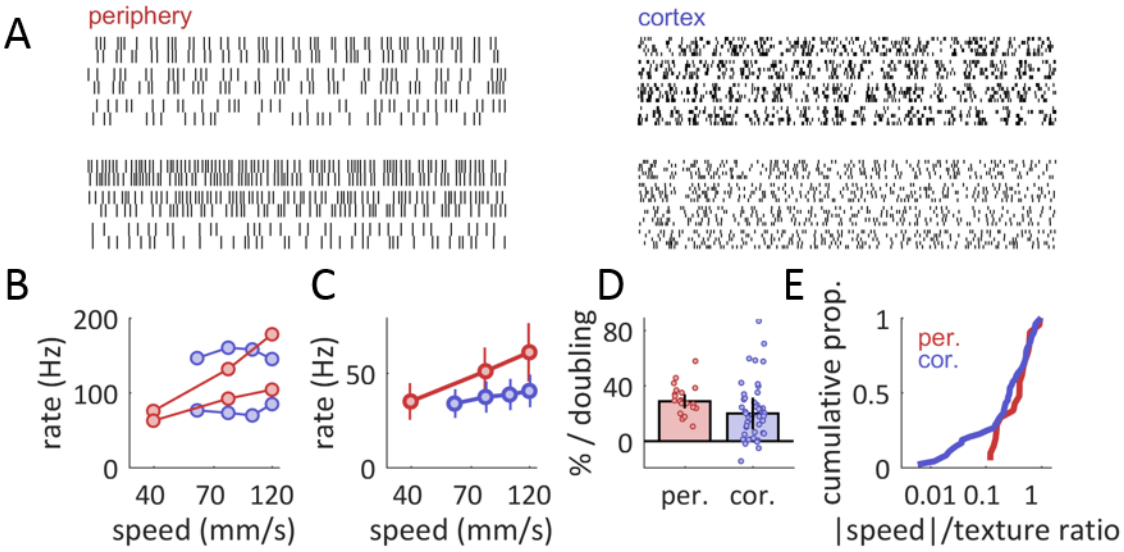

Figure 1. Texture responses are modulated by scanning speed. A| Spiking responses from two example peripheral afferents (top: RA, bottom: PC) and two cortical neurons (top: area 3b, bottom: area 1) to a texture (hucktowel) presented at three/four different speeds, respectively. B| Average firing rate of the spiking response shown in A| for the two afferents (red) and two cortical neurons (blue). C| Average firing rate across all textures and cells at the periphery (red) and in cortex (blue) vs. scanning speed. Error bars denote standard deviations across textures. D| Median speed effect, reported as the percentage increase in mean population firing rate per doubling in speed (normalized to the firing rate at 80 mm/s). Different points denote different neurons. Error bars are median absolute deviations across cells. E| Cumulative distribution of the ratio between the speed effect and texture effect for peripheral afferents (red) and cortical neurons (blue). While the medians of the distributions are similar, the cortical distribution contains a large proportion of strongly speed-independent neurons.

Next, we assessed whether the decreased speed sensitivity in cortex resulted in a more speed-tolerant representation of texture. To this end, we computed the ratio between the texture-dependence of firing rates and their speed dependence (Figure *1E*). The resulting metric, lower for more speed tolerant texture coding – was only marginally lower in cortex than in the periphery (median ratio of speed to texture sensitivity, periphery: 0.59, cortex: 0.47, p=0.287 Wilcoxon rank-sum test), suggesting that cortical texture representations are only slightly more speed tolerant in cortex than at the periphery. Indeed, while speed sensitivity tends to decrease in cortex, so does texture sensitivity. To directly test the ability of individual neurons to discriminate between textures, we computed a signal-to-noise ratio (SNR) as a metric of discriminability for texture pairs (see Methods). However, for any given speed difference, SNR values were largely similar for individual peripheral and cortical neurons (*Supplementary Figure 3A*). Thus, at the single-cell level, speed had a largely similar effect on peripheral and cortical texture responses.

Given that median speed-sensitivity was similar between the peripheral and cortical populations, we next considered whether speed-tolerance might be achieved by a specialized subpopulation of cortical neurons. As signals ascend the somatosensory hierarchy, the tuning of individual neurons becomes increasingly heterogeneous (Lieber and Bensmaia, 2019). We might thus expect subpopulations of cortical neurons to show specialization for speed or texture coding (Bourgeon et al., 2016; Dépeault et al., 2013). Indeed, we found a significant proportion of cortical cells exhibited speed ratios weaker than any observed in peripheral afferents (Figure *1E*) (12/49 with ratio < 0.12, p<0.05, permutation test, see Methods), an effect that was present in all three cortical areas (*Supplementary Figure 2*D). Therefore, somatosensory processing does not simply extinguish speed-sensitivity as signals ascend from the periphery to somatosensory cortex, but rather creates a wide range of response properties in cortex that could potentially represent information about both texture and scanning speed.

Population representations of texture and speed

The diverse tuning of individual cortical neurons suggests that the population representations of texture and speed may be more independent in cortex than at the periphery. To this end, we first identified linear combinations of neurons within each population that best captured either texture-driven modulations (using principal components analysis (PCA) on responses to 24 textures, at a singled speed, namely 80 mm/s) or speed-driven modulations (using demixed principal components analysis (dPCA) (Kobak et al., 2016) on responses to 10 textures, presented at multiple speeds, see Methods). These analyses resulted in two coding spaces for each population (*Figure 2A-B*): a complex texture space consisting of many dimensions (Lieber and Bensmaia, 2019) and a single speed dimension whose projection 1) significantly tracked speed (R^2 to $\log_2$ speed, periphery: 0.64, cortex: 0.24, p < 0.01, F-test) and 2) captured a large proportion of the available speed-related response variance (peripheral: 87.6%, cortical: 63.9%, see Methods).

Next, we examined the relationship between the texture and speed representations by assessing the extent to which changes in one interfered with the other. To this end, we computed the proportion of speed-related variance that was captured by each dimension of the texture representation (*Figure 2C*), a quantity we refer to as the alignment index (Elsayed et al., 2016; Gallego et al., 2018)(see Methods). We found that speed-driven changes were primarily captured by the first principal component of the texture representation and this relationship was far stronger in the periphery than in cortex (average alignment index, peripheral: 0.80, cortical: 0.46). This effect was robust across the full texture space

(*Figure 2D*), where the peripheral representations of texture and speed were still more closely aligned than their cortical counterparts. Surprisingly, this effect was not simply a consequence of a subpopulation of particularly speed-tolerant neurons. Rather, we found that the increased separation of speed and texture was robustly present even when the most speed-tolerant cortical neurons were removed (*Supplementary Figure 4*). We surmised that the increased independence of the cortical texture response could endow it with an increased ability to support speed-independent texture discrimination. We extended our SNR analysis to populations of neurons (see Methods) and indeed found that cortical subpopulations showed stronger discriminability of texture pairs than comparably sized populations of peripheral afferents (*Supplementary Figure 3B-C*), a strong contrast to the largely similar performance seen for individual cortical neurons and afferents. We conclude that, as texture-driven responses ascend the somatosensory hierarchy, populations of neurons encode speed and texture information in increasingly independent representations that support speed-tolerant texture discrimination.

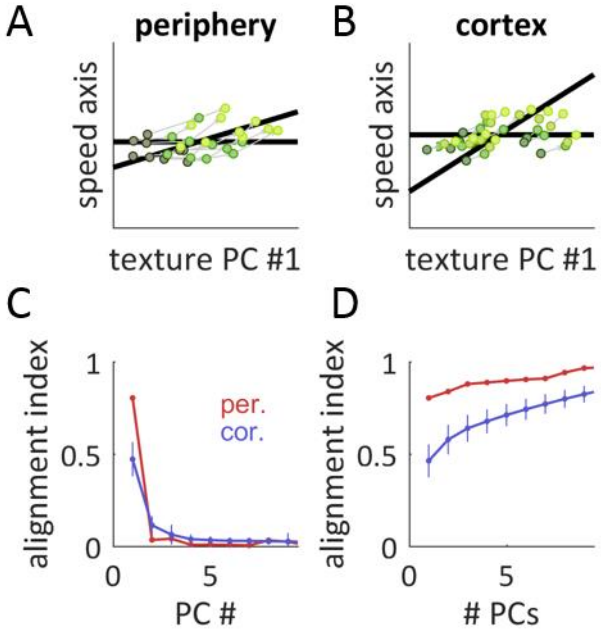

Figure 2. Texture and speed are more independent in cortex than at the periphery. A-B| Texture population responses in plane where one dimension is the first principal component of the texture space (plotted on the abscissa) and the second is the primary speed axis. Texture responses are plotted at three speeds (low speeds: dark green, high speeds: light green). Speed-driven changes in firing rate are less aligned to the primary texture axis in cortex than at the periphery. C| Alignment index between the primary speed axis and individual texture axes for the peripheral (red) and cortical (blue) populations. The alignment index measures the proportion of speed-related variance captured by each texture dimension (see Methods). Error bars for the cortical population (blue) are the standard deviation across randomly sampled subpopulations of 21 neurons. D| Alignment index between the primary speed axis and the multidimensional texture space for the peripheral (red) and cortical (blue) populations, shown for the first 9 principal components of the texture space.

Cortical responses can explain speed-tolerant texture perception

Next, we examined the extent to which neuronal responses could account for the well-documented speed-tolerance of texture perception (Boundy-Singer et al., 2017; Lederman, 1974; Meftah el-M et al., 2000). To this end, we tested the hypothesis that perceived roughness is determined by the population firing rate in somatosensory cortex (Burton and Sinclair, 1994; Lieber and Bensmaia, 2019) using a previously published set of roughness ratings from human subjects. First, we regressed roughness ratings – obtained from human subjects – on to the population firing rate evoked when textures are scanned across the skin at 80 mm/s (*Figure 3A*)(cross validated R^2, peripheral: 0.81, cortical: 0.77). Next, we assessed how well this linear model could account for the neuronal responses at other speeds (*Figure 3B*). We found that roughness estimated from both peripheral and cortical responses were strongly modulated by changes in scanning speed (% increase in roughness per doubling of speed, periphery: 29.9%, cortex: 19.4%) in contrast to the roughness ratings, which were largely speed-independent. Given the observed heterogeneity of cortical tuning, we next considered that the neural code for roughness might rely more on some neurons than others (Bourgeon et al., 2016; Chapman et al., 2002). To test this hypothesis, we regressed the main texture-related principal components of each population response on perceived roughness (*Figure 3A-B*, middle bars). Using additional regression parameters led to a more accurate prediction of perceived roughness (cross-validated R^2, peripheral: 0.87, cortical: 0.81), but only marginally reduced the speed dependence of the roughness predictions (% increase in roughness per doubling of speed, periphery: 25.8%, cortex: 15.3%).

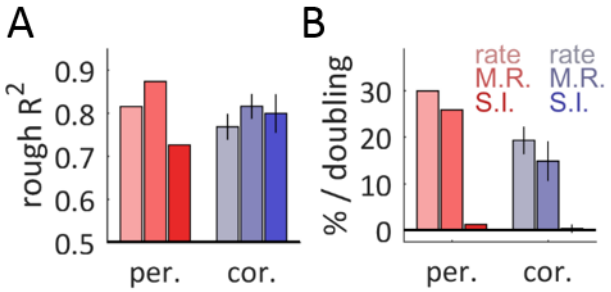

Figure 3. Cortex encodes a speed-tolerant representation of perceived roughness. A| Cross-validated R^2 between the predicted and true roughness, for predictions based on peripheral (red) and cortical (blue) population responses (populations of 21 cells). From left to right, bars represent predictions based on regressions of the population averaged firing rate (light, rate), the best-fit regression of 5 principal components (medium, M.R.), and a best-fit regression constrained to minimize speed dependence (dark, S.I.). Error bars denote standard deviations across different samples of 21 cells. B| Speed dependence of the roughness prediction reported as a percentage increase in firing rate per doubling of speed, with color conventions as in A| The cortical population can support a speed-independent prediction of roughness, while the peripheral population cannot simultaneously support speed-independence and an accurate roughness prediction.

To create fully speed-independent roughness predictions, we next constrained our regression weights to be orthogonal to the primary speed-related dimension in each population (*Figure 3A-B*, right bars)(found using dPCA, as above). This approach successfully eliminated the speed-dependence for

both sets of roughness predictions (% increase in roughness per doubling of speed, periphery: 1.2%, cortex: 0.2%). However, for the peripheral population, enforcing speed-independence strongly reduced the predictive power of the peripheral model (peripheral cross-validated R^2: 0.73, from 0.87). In contrast, enforcing speed independence had essentially no effect on the predictive power of the cortical model (cortical cross-validated R^2: 0.79 from 0.81). This effect was robust across a wide range of subpopulation sizes and regression parameters (*Supplementary Figure 5*). Thus, the cortical population response contains a speed-independent readout of perceived roughness that is not present in the peripheral firing rate response.

Known cortical computations account for the untangling of speed and texture information

As information ascends any sensory neuraxis, neural representations are repeatedly transformed by a set of canonical computations that shape the feature selectivity of downstream neurons. One well-established transformation in the somatosensory system is the calculation of spatial (Connor and Johnson, 1992; DiCarlo and Johnson, 2000; Lieber and Bensmaia, 2019) and temporal (Saal et al., 2015) variation: the extent to which the peripheral neural representation exhibits inhomogeneous ("edge-like") structure in space or time. We hypothesized that these differentiation computations could also give rise to an increasingly heterogeneous population response to texture and speed as signals ascend from periphery through cortex. Indeed, increased response heterogeneity has been proposed as an organizing principle for the structure of receptive fields in the visual and auditory systems (Van Hateren and Ruderman, 1998; Lewicki, 2002; Olshausen and Field, 1996, 2004). To test this hypothesis, we built a neurally plausible model of spatial and temporal variation using the responses of peripheral afferents (*Figure 4A*, see Methods). Using a range of biologically plausible model parameters (see Methods), we investigated whether pseudo-populations of modeled "downstream" neurons exhibited speed-tolerant texture coding.

We first verified that the outputs of the variation model resembled actual cortical responses to texture (median correlation with population-averaged cortical response to 24 textures scanned at 80 mm/s: variation model outputs r=0.71, individual cortical neurons r=0.75). Next, we evaluated the speed-sensitivity of individual "downstream" model outputs by calculating their speed/texture sensitivity ratio (as above). Outputs of the variation model showed comparable levels of speed-sensitivity as did peripheral afferents (*Figure 4B*)(speed ratio, median ± median absolute deviation, model: 0.43±0.18 vs. afferents: 0.59±0.18). However, when we examined population-level representations in model outputs using the texture/speed alignment index (as above), we found that small populations separated texture and speed representations more robustly than did peripheral afferents (*Figure 4C*). Our modeling results suggest that the well-established cortical computations of spatial and temporal differentiation contribute to the heterogeneous speed- and texture-sensitivity observed in somatosensory cortex, which in turn underlies the untangling of speed and texture representations.

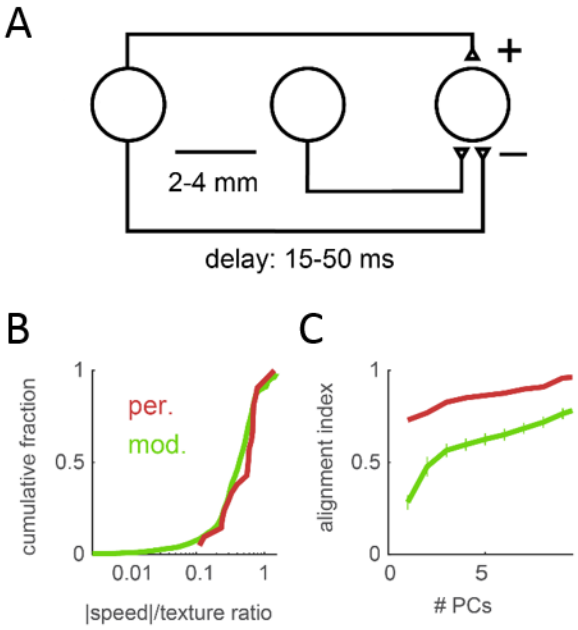

Figure 4. Cortical differentiation mechanisms can account for the separation of speed and texture information. A| Cartoon of the variation model. The texture response of a single afferent is combined with a spatial variation signal, modeled as an inhibitory response coming from a different afferent located 2 to 4 mm away in the scanning direction, and a temporal variation signal, modeled as an inhibitory copy of the original afferent's response delayed by 15-50 ms. B| Cumulative distribution of the ratio between the speed effect and texture effect for peripheral afferents (red) and variation model outputs (green). C| Alignment index (as in Figure *2*) between the speed and texture spaces for populations of peripheral afferents (red) and model outputs (green), shown for the first 9 principal components of the texture space. Error bars denote the standard deviation across subsamples of model outputs. The variation model exhibits a greater separation of speed and texture information than does the afferent population.

DISCUSSION

The perception of texture is remarkably tolerant to changes in scanning speed. Indeed, psychophysical ratings along the three principal perceptual axes of textures – roughness, hardness, and stickiness – are identical across speeds (Boundy-Singer et al., 2017; Lederman, 1974; Meftah el-M et al., 2000). Furthermore, the perceived dissimilarity of a pair of textures – which probes texture perception across all of its dimensions and attributes – is very similar whether the two textures are scanned at the same speed or at different speeds (Boundy-Singer et al., 2017). What makes this tolerance so remarkable is that the response of tactile nerve fibers are highly speed dependent. Indeed, in the nerve, texture-elicited firing rates increase with scanning speed, and temporal spiking sequences, which carry critical texture information, also change with speed. The central result of the present study is that the cortical population response exhibits a capacity for speed-tolerant coding of texture that exceeds the capabilities of the peripheral population response. Therefore, somatosensory processing between the

periphery and cortex yields overlaid representations of texture and speed that are relatively independent, and thus much easier to decode independently.

Validity of the macaque model for human texture perception

In the present study, we use neural responses measured in macaques to predict human texture perception. Human and macaque hands show very similar patterns of cutaneous innervation (Darian-Smith and Kenins, 1980; Johansson and Vallbo, 1979; Paré et al., 2003) and the tactile nerve fibers in the two species exhibit nearly identical response properties (Johansson et al., 1982; Phillips et al., 1992). Human texture perception can be successfully predicted by the responses of macaque nerve fibers (Blake et al., 1997; Connor and Johnson, 1992; Connor et al., 1990; Lieber et al., 2017; Weber et al., 2013) and cortical neurons (Bourgeon et al., 2016; Lieber and Bensmaia, 2019).

Previous work on speed tolerance of texture representations

We find a continuum of response properties in somatosensory cortex, from neurons that are as sensitive to speed as are peripheral afferents to neurons that are nearly speed-independent. These data are broadly consistent with previous studies that have emphasized that different cortical neurons show responses that are purely texture-selective, purely speed-selective, or responsive to both texture and speed (Bourgeon et al., 2016; Dépeault et al., 2013; Tremblay et al., 1996). However, we emphasize that there exists significant response heterogeneity within these subpopulations as well, and that the distribution of speed-sensitivity across cortex is likely better described as a continuum than as a bimodal distribution of texture and speed specialists.

Variation filters create speed-tolerant representations of texture

In the above analyses, we compare texture representations in afferent firing rates and cortical firing rates. However, a large body of evidence suggests that stimulus information is not encoded simply in the firing rates of tactile nerve fibers, but rather in spatio-temporal patterns of activation (Birznieks and Vickery, 2017; Connor and Johnson, 1992; DiCarlo and Johnson, 2000; LaMotte and Mountcastle, 1975; Mackevicius et al., 2012; Talbot et al., 1968; Weber et al., 2013). These putative peripheral neural codes imply computations along the neuraxis where spatio-temporal motifs in the afferent input are converted to firing rate codes downstream. One of the canonical computations is that of differentiation, both spatial and temporal. Indeed, neurons in somatosensory cortex have been shown to exhibit Gabor-like spatial receptive fields, reflecting a spatial differentiation (Bensmaia et al., 2008; DiCarlo and Johnson, 2000; Sripati et al., 2006), and bi-lobed temporal receptive fields, reflecting temporal differentiation (DiCarlo and Johnson, 2000; Saal et al., 2015; Sripati et al., 2006). We demonstrate that these computations confer an additional benefit to the cortical code for texture: increased separability of representations for texture and speed. This separability likely reflects a broader sensory function, namely to create a basis set that efficiently and sparsely encodes behaviorally relevant features across the breadth of naturally occurring stimuli (Olshausen and Field, 2004). In the somatosensory system, Gabor-like spatial and temporal filters transform a largely homogeneous set of peripheral responses into a widely divergent set of cortical responses, as has also been shown in the visual system (Van Hateren and Ruderman, 1998; Olshausen and Field, 1996).

Tolerance as a canonical sensory computation

To produce a stable percept of object identity, the somatosensory system must remove the influence of speed from the texture representation. However, information about tactile speed is behaviorally relevant, and thus ideally would be preserved rather than eliminated. We find that the somatosensory system does not throw speed information away, but rather partitions texture and speed representations into increasingly separated subspaces. This partitioning is not perfect: the representation of tactile speed in somatosensory cortex is highly contaminated by texture identity and this influence of texture leads to a predictably non-veridical perception of tactile speed (Delhaye et al., 2019). Nonetheless, the preservation of any speed information speaks to the capacity of the cortical population representation to simultaneously encode many relevant variables simultaneously.

We find that, at the somatosensory periphery, object information (texture) and information about exploratory parameters (speed) are inextricably tangled together. As this mixed signal ascends the somatosensory hierarchy, it is transformed into two independently readable representations of these two parameters. This mirrors results from vision and audition, where successive levels of processing lead to a higher fidelity readout of both object identity (Rust and DiCarlo, 2010; Town et al., 2018) and exploratory parameters (Hong et al., 2016). These convergent results suggest that separating (or untangling) information about objects and exploratory parameters is a canonical sensory computation (DiCarlo and Cox, 2007).

METHODS

Experimental Methods

Peripheral texture responses

The methods for recording afferent responses to textured stimuli have been previously described in detail (Lieber et al., 2017; Weber et al., 2013). In brief, we recorded the responses of tactile fibers to 55 textured surfaces scanned over the fingertip, including everyday textures such as fabrics, sandpapers, as well as plastic gratings and embossed dots. We analyzed the texture responses of a subset of 21 afferents (9 SA1, 9 RA, and 3 PC fibers) from which we had responses at 3 different scanning speeds, namely 40, 80, and 120 mm/s (all ± 0.1 mm/s, at least 1, 2, and 3 repetitions at each speed, respectively). Recordings were collected from afferents innervating the distal fingertip in the median and ulnar nerves, using standard methods (Talbot et al., 1968). Anesthesia was maintained using isoflurane.

In these experiments, texture presentation was blocked by speed rather than by texture. That is, we first recorded the response of afferents to all 55 textures at 80 mm/s, then at 40 mm/s or 120 mm/s, and in the third block at the remaining speed. Our analyses only consider responses during the steady-state contact period for force and speed, which lasted for at 2, 1, and 0.5 seconds, at 40, 80, and 120 mm/s, respectively.

Cortical texture responses

The methods for recording the responses evoked in the somatosensory cortex of macaques to textured surfaces scanned across the fingertip have been previously described in detail (Lieber and Bensmaia, 2019). In brief, extracellular recordings were made in the postcentral gyri of three hemispheres in each of three awake macaque monkeys (all male, 6-8 yrs old, 8-11 kg). On each recording day, a multielectrode microdrive (NAN Instruments, Nazaret Illit, Israel) was loaded with three electrodes

(tungsten, Epoxylite insulated, FHC Inc.), spaced 650-µm apart, which were driven into cortex until they encountered neurons from Brodmann's areas 3b, 1, and 2 of with RFs on the distal fingerpad of digits 2-5. The respective cortical fields were identified based on anatomical landmarks, RF location, and response properties. Recordings were obtained from neurons that met the following criteria: (1) action potentials were well isolated from the background noise, (2) the finger could be positioned such that the textured surface impinged on the center of the RF, and (3) the neuron was clearly driven by light cutaneous touch. Isolations had to be maintained for at least 30 minutes to complete 5 repetitions of the basic texture protocol (59 different textures presented at 80 mm/s) and an additional 25 minutes to complete 5 repetitions of the speed protocol (10 different textures presented at 4 different speeds).

Responses from 141 single units were obtained for the basic texture protocol: 35 units from area 3b, 81 units from area 1, and 25 units from area 2. 49 of these single units were held long enough to obtain responses for the speed protocol: 14 units from area 3b, 26 units from area 1, and 9 units from area 2. In this protocol, ten textures were presented at 4 different speeds: 60, 80, 100, and 120 mm/s (all ± 1.1 mm/s). Four of these textures (satin, chiffon, nylon, and hucktowel) were also used in our recordings of afferent responses (see below) and 6 were not (fabric grating [wide spacing], sunbrella upholstery, fuzzy upholstery, faux croc skin, 7.7 mm dots, 7.7 mm dots / 1 mm grating overlay). The order in which scanning speed was selected was pseudo-random for each texture and each texture was presented 5 times at each speed, for 2.3, 1.7, 1.4, and 1.2 seconds at 60, 80, 100, and 120 mm/s, respectively.

Roughness magnitude estimation

We reanalyzed roughness magnitude estimation data previously described in detail (Lieber and Bensmaia, 2019). Briefly, 6 subjects (5m, 1f, ages 18-24) were passively presented with each of 59 textures presented at 80 mm/s and produced a rating proportional to its perceived roughness. This procedure was repeated 6 times over 6 blocks. Ratings were normalized within block and then averaged within subject. Because ratings were consistent across subjects (correlation: 0.87 ± 0.079), ratings were then averaged across subjects. All procedures were approved by the Institutional Review Board of the University of Chicago and all subjects provided informed consent.

Analysis

Firing rates and speed effects

Peripheral firing rates were calculated over windows of 2, 1, and 0.5 seconds for textures presented at 40, 80, and 120 mm/s, respectively. Cortical firing rates were calculated over windows of 2.3, 1.7, 1.4, and 1.2 seconds for textures presented at 60, 80, 100, and 120 mm/s, respectively. All cortical firing rates were corrected for baseline firing. For each neuron, firing rates were calculated over a 500 ms period before texture contact, and then averaged over trials, textures, and speeds to get a single baseline firing rate. This baseline rate was then subtracted that neuron's raw cortical firing rates.

We noted that the speed-sensitivity of any given neuron could differ depending on which texture was presented. To minimize any systematic biases due to differences in the texture set, we selected a set of 10 peripheral textures to match the 10 textures used in the cortical experiment. Four (4) of these textures were used in both experiments, so we sought to find appropriate matches for the remaining 6. We looked within a subset of 20 textures for which we had cortical responses at 80 mm/s and peripheral responses at all three speeds. To assess similarity between the speed-set of 6 textures and the shared

set of 20 textures, we calculated distances between texture pairs (6*20=120 pairs) based on the Euclidean distance between trial-averaged firing rate responses of the cortical neuronal population and then iteratively picked the 6 pairs with the smallest distance. For all analyses in the manuscript, we achieved qualitatively similar results when we used peripheral responses from the full set of 55 textures.

To quantify the effect of speed on texture-driven firing rates, we calculated a linear regression between the log (base 2) of presentation speed and firing rate. The results of our study were relatively insensitive to using either linear units or log units for presentation speed. We opted towards log units for two reasons. First, we noted that firing rate differences at the lowest speeds (40 mm/s and 80 mm/s at the periphery, 60 mm/s and 80 mm/s in cortex) tended to be larger than firing rate differences at higher speeds. Second, using log units tends to produce shallower slopes for the peripheral data (due to the wider range of speeds used in that experiment), and thus provides a more conservative estimate of the difference in speed-sensitivity between the two areas.

Calculating speed-sensitivity, speed ratio, and response heterogeneity

We wished to quantify the relative effect of speed and texture on each afferent and neuron. To this end, we calculated three quantities for each cell. First, we defined speed-sensitivity as the slope of the linear regression between log speed and firing rate, normalized by the mean firing rate at 80 mm/s of the 10 textures used in the regression. Second, we defined texture-sensitivity as the cross-texture coefficient of variation: that is, the standard deviation across the firing rate responses to 24 textures presented at 80 mm/s, normalized by the average firing rate of those same 24 textures. Finally, we defined the speed ratio as the ratio of speed-sensitivity to texture-sensitivity. We report that the cortical population has a significant proportion of neurons with a smaller speed ratio than any peripheral afferent. To test the significance of this effect, we randomly shuffled the cortex/periphery labels on the combined population of afferents and cortical neurons 200,000 times, and recomputed the number of "neurons" with smaller speed ratios than "afferents," to compute the distribution of smaller speed ratios we would expect by chance.

Neural population analyses

We sought to evaluate the extent to which representations of texture and speed in the neural populations were either overlapping or well-separated. This required a three step process: 1) identify the texture representation in each population, 2) identify the speed-representation in each population, and 3) determine the amount of overlap between the two representations.

To identify the major axes of each population's texture response, we applied a principal components analysis (PCA) to peripheral and cortical population responses, using only the responses to the set of 24 textures (presented at 80 mm/s) shared between the two data sets. This allowed us to identify the first D dimensions in each population that captured the majority of the texture response variance, which we refer to as P_t. To identify the main speed-related axis in each population, we applied demixed principal components analysis (dPCA) (Kobak et al., 2016) to the full set of trial-averaged responses to textures presented at multiple speeds (periphery: 10 textures at 3 speeds, cortex: 10 textures at 4 speeds). Specifically, we first created a speed-marginalization of the population response by subtracting out each texture's average firing rate (across all speeds) from the full response matrix. Thus, the full response matrix can be expressed as:

$$X = X_t + X_s$$

where X is the full texture response, X_t is the texture marginalization, and X_s is the speed marginalization (which, in the terminology of (Kobak et al., 2016), contains both the pure speed marginalization and speed-texture interaction marginalization). Next, we found the best linear mapping from the full texture response to the speed marginalization using least squares regression:

$$A = X_s X^T (XX^T + \lambda^2 \mu_N I)^{-1}$$

where λ is a regularization parameter (set to 10^{-6}, as in (Kobak et al., 2016)) and μ_N is each neuron's variance across all speed and texture conditions. Finally, we used PCA on the best linear approximation of the speed marginalization, AX, to find its primary axis of variation, which we refer to as P_s. In the terminology of (Kobak et al., 2016), this corresponds to the primary encoder axis for the speed marginalization.

We validated each population's primary speed-axis using two metrics. First, we confirmed that the projection of any given population response onto the speed axis covaried with the actual speed (in log units) by measuring the coefficient of determination between the two variables (periphery: 10x3=30 conditions, cortex: 10x4=40 conditions). Second, we quantified the extent to which the primary speed-axis could explain speed-driven neural responses as a ratio of variances: the variance captured by the single speed axis divided by the full amount of variance in the speed marginalization (summed across neurons).

To determine the amount of overlap between the texture space and the speed dimension, we calculated an alignment index (Elsayed et al., 2016; Gallego et al., 2018), which we defined as the amount of speed-driven variance captured by the texture space, normalized by the total amount of speed-related variance in the population response. Specifically, we define the alignment index as:

$$AI = \frac{Tr\big(Cov(P_t X_s)\big)}{Tr\big(Cov(X_s)\big)}$$

where P_t is defined as the principal axes of the texture space. We emphasize that, by construction, this metric is insensitive to the raw magnitude of speed-related fluctuations in the population response. We verified with simulations that when the speed ratio of the population response is doubled or halved the alignment index stays constant. In this sense, the alignment index is more similar to a relative angle between to representations than to a measurement of raw speed-sensitivity. For Figure *2*, we recomputed the texture-space, speed-axis, and alignment index for different subsamples of 21 neurons within the cortical space (to control for systematic biases due to sample size), for either individual dimensions of P_t (Figure *2*A), and for a range of the first D dimensions of P_t (Figure *2*B).

Texture discriminability across changes in speed

We sought to quantify how well populations of neurons could discriminate pairs of textures, and to what extent discrimination was impaired by noise due to changes in speed. For an individual neuron responding to any pair of textures and pair of speeds, we define a signal-to-noise ratio:

$$SNR = \frac{\left(r_{t1,s1} + r_{t1,s2}\right) - \left(r_{t2,s1} + r_{t2,s1}\right)}{\left|r_{t1,s1} - r_{t1,s2}\right| + \left|r_{t2,s1} - r_{t2,s2}\right| + 1}$$

where $r_{t1,s1}$ is the firing rate response of a neuron to a texture t_1 at speed s_1. Because some neurons fire no spikes to either texture in some conditions, we add 1 in the denominator to avoid unrealistically large SNR values. To compute SNR for populations of neurons, we project the population firing rates R onto the line connecting the mean firing rates of each texture $\left(R_{t1,s1} + R_{t1,s2}\right) - \left(R_{t2,s1} + R_{t2,s1}\right)$. We then compute SNR on these projections in place of the rates.

Predicting roughness from neural responses

We sought to evaluate how well neural population responses could predict human judgements of surface roughness (55/59 textures for periphery and cortex, respectively, all presented at 80 mm/s). To this end, we implemented three distinct models: a mean firing rate regression model, a multiple regression model, and a constrained multiple regression model. The mean firing rate model was fit using a single regressor, the mean firing rate across the full population of neurons (21 afferents, 49 cortical neurons). The multiple regression model was fit using the first N principal components of the texture representation. For Figure 5, we chose a number of principal components where regression performance began to saturate (N=5), though the results were stable over different numbers of components (*Supplementary Figure 5*). To build a speed-tolerant prediction of roughness, we first find the primary speed axis in each population using dPCA (described above). Next, we remove the speed-axis projection from the full set of population firing rates. Finally, we perform the multiple regression as described before. This methodology ensures that the final regression weights will be orthogonal to the primary speed axis.

For all three models, we use leave-one-out cross-validation to compute an equivalent of the coefficient of determination (R^2). Specifically, for each texture in the set, we first fit the model using the other 23 texture responses as training data. We then applied that model to produce a prediction of roughness magnitude $\widetilde{m_t}$ for the final, left-out texture. Across all textures, we compute the coefficient of determination as:

$$R^2 = 1 - \frac{\sum_t (m_t - \widetilde{m_t})^2}{\sum_t (m_t - \bar{m})^2}$$

where m_t is the reported roughness.

To test the speed-tolerance of these models, we applied each model (now fit on the full set of 55/59 textures) to texture responses at multiple speeds (10 textures in each set). We computed speed-sensitivity of the roughness predictions in a manner similar to that used for the neural data. First, we compute the slope of roughness (averaged across textures) vs. speed ($\log_2$ units). Then, we normalize the slopes by the average predicted roughness magnitude at 80 mm/s. Thus, as with the neuronal data, we report the speed-sensitivity of the roughness predictions as a percentage increase per doubling of speed.

Modeling spatial and temporal variation

As somatosensory information ascends from the periphery to cortex, spatiotemporal patterns of peripheral population activity are transformed by spatial and temporal variation filters (Connor and Johnson, 1992; DiCarlo and Johnson, 2000; Saal et al., 2015). We built a simple model of these filters by combining the responses of peripheral afferents to textures presented at multiple speeds. Specifically,

we first temporally smoothed afferent spike train responses using an EPSP-like filter (Bengtsson et al., 2013):

$$EPSP(t) = A * H(t - t_0)e^{-t/\tau}$$

where t_0 is the time of each spike, τ is a decay time set to 5 ms, $H(t)$ is the Heaviside step function, and A is a normalization constant such that $\int dt\ EPSP(t) = 1$. The integration time of temporally lagged inhibition is generally longer than that of excitation (DiCarlo and Johnson, 2000; Sripati et al., 2006), so for the temporal variation inhibition field (see below) we recomputed spike trains with τ set to 9 ms.

Using these traces we sought to create a large population of temporally aligned peripheral spike trains, which would allow us to use specific temporal offsets to simulate temporal or spatial gaps for the variation computation. For each texture and speed, we aligned all the trial-averaged traces in the population (between 21 and 39 neurons, depending on the speed) iteratively by first finding the strongest cross-correlation between any two pairs of neurons (within a maximum shift of 300 ms), averaging them at their optimal lag, and then finding the strongest cross-correlation between this new trace and any of the remaining traces. This was repeated until the full population was maximally aligned. As we only had one 2-second trace for any given texture responses at 40 mm/s, these traces were split in half and then maximally aligned to create two 1-second traces.

Next, we computed pseudo-populations of "downstream" neurons that implement both spatial and temporal variation filters. For each individual "downstream" neuron, we first started with the smoothed spike train of a single afferent. We implemented temporal variation by subtracting out a delayed version of the same spike train (this time smoothed over 9 ms), at random delays (sampled evenly between 15 and 50 ms) and weights (0 to 50% of the excitatory weight) that are consistent with previous literature on cortical spatial-temporal receptive fields (DiCarlo and Johnson, 1999, 2000; Saal et al., 2015; Sripati et al., 2006). We implemented spatial variation by subtracting out the response of a different, randomly selected afferent of the same type (that is, matched as SA1, RA, or PC). We simulated the spatial location of the inhibitory subfield as a trailing (relative to the scanning direction) between 2 and 4 mm (randomly selected) behind the excitatory subfield at a random weight (0 to 50% of the excitatory weight), again consistent with previous literature (DiCarlo and Johnson, 1999, 2000; Sripati et al., 2006). In practice, this meant subtracting out the spatial inhibition at a temporal delay that shifted for different speeds. After subtracting out both the temporal and spatial inhibition, we then half-wave rectified each trace and averaged the trace to get an "output" value for each set of inputs. This procedure was repeated for two trials of every texture response at every speed, and then repeated 100 times for each afferent, each time for a different selection of the randomized parameters; thus, for every individual afferent we created a matched set of corresponding "downstream" neurons, each with their own response to textures at different speeds.

For each of these "downstream" neurons, we computed two quantities: the correlation of its outputs at with those from the population averaged cortical response (24 shared textures, 80 mm/s, all 141 neurons), and the speed/texture ratio of its outputs (as defined above). The median correlation reported in the text and the cumulative distribution in *Figure 4A* were computed across all permutations and afferents. To find the alignment index for populations of "downstream" neurons, we first randomly selected a single model output from each afferent's corresponding group to get a population of 21 total

"neurons." We then computed the alignment index on this pseudo-population as above. We repeated this procedure over 200 random selections of the downstream population.

SUPPLEMENTARY FIGURES

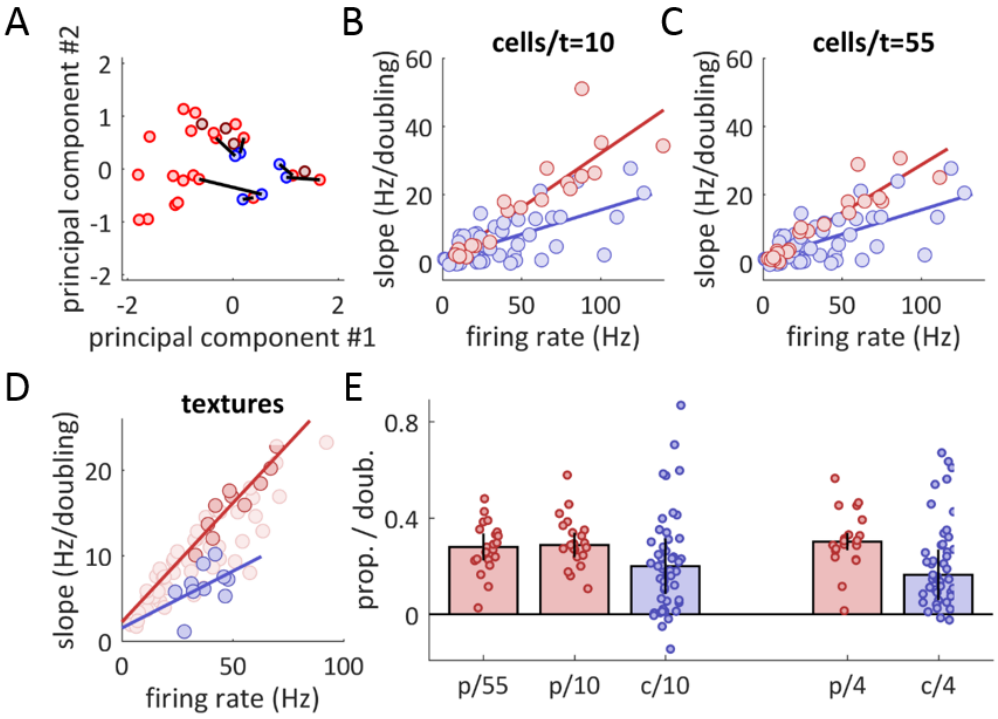

Supplementary Figure 1. Speed-driven increases in firing rate are proportional to average firing rate. A| Cortical population responses to 30 different textures were projected onto the first two principal components of the texture representation (all presented at 80 mm/s). Four (4) of these textures were included in the speed set for both experiments (purple), twenty textures were included in the peripheral speed set but not the cortical one (red), and 6 textures (blue) were included in the cortical speed set but not the peripheral one. To fairly compare analyses from the periphery and cortex, we found the 6 textures from the peripheral speed set that evoked cortical responses most similar to the 6 non-overlapping textures from the cortical speed set (black lines). This set of 6 textures (combined with the set of 4 overlapping textures) was used for all analyses. B| Speed sensitivity of individual neurons (measured in Hz / doubling of speed) vs. that neuron's mean firing rate across textures, for peripheral afferents (red, using the set of 10 matched textures) and cortical neurons (blue). Each point denotes a cell. Speed slopes increase proportionally to each neuron's average excitability (F-test for regression fit, both $p<10^{-6}$). C| Speed sensitivity vs. mean firing rate across textures as in B|, but afferent response are averaged over the full set of 55 textures (F-test for regression fit, both $p<10^{-6}$). Results are similar regardless of the texture set used. D| Population speed sensitivity vs. mean firing rate across neurons, for individual textures. Dark red points indicate the matched peripheral set of 10 textures, light red indicate the other 45 textures. While peripheral slopes are closely related to the averaged population firing rates (F-test for regression fit, $p<10^{-3}$), cortical slopes show a much noisier relationship ($p=0.19$). Different points denote different textures. E| Median normalized speed sensitivity for the peripheral and cortical population, averaged over different sets of textures. Peripheral data is averaged over either the full set of 55 textures, the matched set of 10 textures, or the exactly overlapping set of 4 textures. Cortical data is averaged over the full set of 10 textures or the overlapping set of 4 textures. Cortical slopes are consistently lower than peripheral slopes, regardless of the texture set used to compute them.

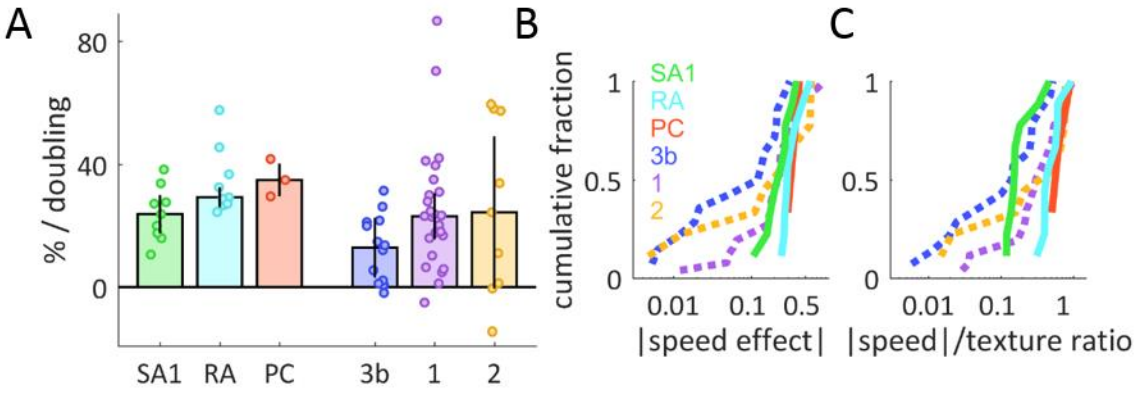

Supplementary Figure 2. Speed sensitivity differs across afferent classes and cortical fields. A| Speed sensitivity for afferents and cortical neurons, broken out by afferent submodality and cortical area. Neurons in area 3b trend towards less speed-sensitivity than those in area 1 (p<0.05) or area 2 (p=0.33). B| Cumulative distribution of speed-sensitivity (absolute value) across afferents and neurons (same data as in A|, replotted). Colors represent afferent submodality and cortical area, as in A|. C| Cumulative distribution of the ratio between speed-sensitivity (as in B|) and texture coefficient of variation for each afferent and cortical neuron. All three cortical areas show a significant subpopulation of neurons that are more speed-tolerant than the most speed-tolerant SA1 afferent (fraction of neurons with a speed/texture ratio less than the lowest SA1 ratio: area 3b: 6/14, area 1: 4/26, area 2: 2/9, all p < 0.05).

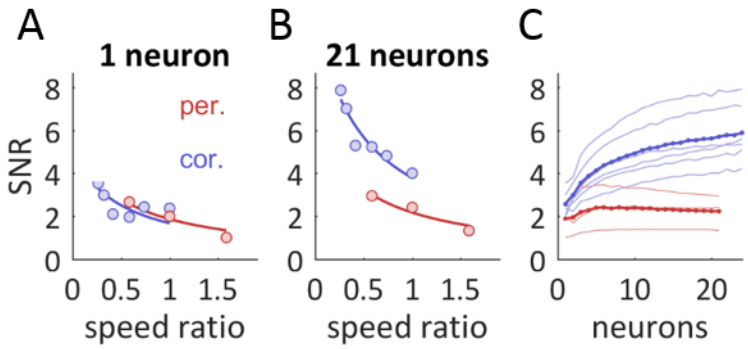

Supplementary Figure 3. The cortical population representation of texture is more tolerant to changes in speed than the peripheral representation. A| SNR vs. speed ratio, averaged across all texture pairs (10 textures) for peripheral afferents (red) or cortical neurons (blue). We defined SNR as the difference in response to each texture, averaged across a pair of speeds (the "signal") divided by the spread of each texture's firing rate across speeds (the "noise"). SNR was calculated over mean firing rates at two speeds which could be close together (left) or far apart (right). Best-fit curves of the form $A/(0.5+x)$ were fit to the data (see Methods). As expected, larger differences in speed drove lower discriminability for both tactile nerve fibers and cortical neurons, but discriminability is similar between the two populations at any given difference in speed. B| SNR vs. speed difference, now in multidimensional space for groups of 21 neurons. Discriminability was calculated along the neural dimension connecting the centers of the two textures. C| SNR vs. group size for individual conditions (light colors) and averaged across conditions (dark colors). Peripheral discriminability saturates quickly, while cortical discriminability grows rapidly for all conditions.

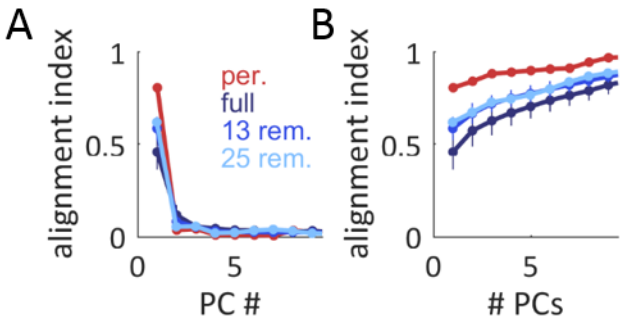

Supplementary Figure 4. Cortical separation of texture and speed representations is robust even among the most speed-sensitive subpopulations. A| Alignment index between the primary speed axis and individual texture axes, as in Figure 3C for three cortical subpopulations: the full cortical population (dark blue), a cortical population with the 13 most speed-tolerant cells removed (medium blue, tolerance measured using speed ratio, as in Figure 2B), and a cortical population with the 25 most speed-tolerant cells removed (light blue). B| Alignment index between the primary speed axis and the multidimensional texture space, as in Figure 3D. Colors as in A|. Even when the analysis is confined to the most speed-sensitive neurons, the cortical population response still shows more separation between speed and texture than does its peripheral counterpart.

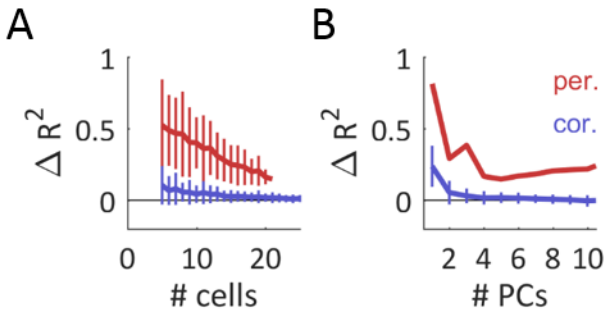

Supplementary Figure 5. Models for predicting perceived roughness. A| Difference in cross-validated R^2 between the full multiple regression model and the regression model constrained to be speed-independent, for neuronal subpopulations of different sizes (peripheral afferents: red, cortical neurons: blue). Each regression model was constrained to use the first 5 principal components of the population response – as such, we only plot results for subpopulations of size 5 and larger. B| As above, difference in cross-validated R^2 between the two model classes, now for regression models trained using different numbers of principal components. All models were trained on subpopulations of 21 neurons. Cortical regression models were consistently more robust to the imposition of speed-independence.

Paper	Neural Subpopulation	Slope	Notes
Goodwin and Morley 1987a	SA1	~ 0%	Gratings, sinusoidal motion
	RA	23%	Gratings, sinusoidal motion
	PC	28%	Gratings, sinusoidal motion
Phillips and Johnson 1994	Human SA1	24%	2 mm spaced dot pattern
	Human RA	22%	2 mm spaced dot pattern
Essick and Edin 1995	Human, unspecified Aβ afferent	14%	Brush stroked over RF
DiCarlo and Johnson 1999	SA1	17%	Random dot pattern
	RA	30%	Random dot pattern
	Cortical: 3b	14%	Random dot pattern
Sinclair and Burton 1991	Cortical: 3b & 1	14%	Actively scanned texture, scans at higher velocity were correlated with lower applied normal force
Dépeault et. al. 2013	Cortical: 3b, 1, and 2	28%	Data from a subset of cortical neurons that exhibited statistically significant speed modulation

Supplementary Table 1. Previous published results on speed sensitivity at the periphery and in cortex. Firing rate responses from previous studies were re-fit using the speed-sensitivity metric described in this paper (slope of the linear fit in $\log_2$(speed) coordinates). Results from (Goodwin and Morley, 1987a) are based on the peak speeds of sinusoidal, back-and-forth sweeps, measured for a range of different periodic grating textures. Results from (Essick and Edin, 1995) are in response to a brush sweeping over the skin, rather than a classically defined texture. Neural responses from (Sinclair and Burton, 1991) were in response to macaque monkeys actively scanning textures with their finger (in contrast to the passive presentation of texture used in the other cited studies). As a result, the velocity and force used to scan the texture were under the volitional control of the animal, and thus 1) not consistent trial-to-trial and 2) negatively correlated across trials. That is, unlike scans in the passive condition, scans at higher velocities tended to use less force. This may help explain the slightly lower levels of observed speed-sensitivity. Finally, the firing rate responses reported in (Dépeault et al., 2013) are not from the full population of somatosensory cortical neurons – rather, the authors only report the effect size of speed-modulation from the subset of neurons where that effect reaches statistical significance. This may help explain the slightly higher levels of observed speed-sensitivity. Overall, the levels of speed-sensitivity found in the present study broadly line up with those observed in previous work.

REFERENCES

Avidan, G., Harel, M., Hendler, T., Ben-Bashat, D., Zohary, E., and Malach, R. (2002). Contrast sensitivity in human visual areas and its relationship to object recognition. J. Neurophysiol. *87*, 3102–3116.

Bengtsson, F., Brasselet, R., Johansson, R.S., Arleo, A., and Jörntell, H. (2013). Integration of Sensory Quanta in Cuneate Nucleus Neurons In Vivo. PLoS One *8*.

Bensmaia, S.J., Denchev, P. V, Dammann, J.F., Craig, J.C., and Hsiao, S.S. (2008). The representation of stimulus orientation in the early stages of somatosensory processing. J. Neurosci. *28*, 776–786.

Birznieks, I., and Vickery, R.M. (2017). Spike Timing Matters in Novel Neuronal Code Involved in Vibrotactile Frequency Perception. Curr. Biol. *27*, 1485-1490.e2.

Blake, D.T., Johnson, K.O., and Hsiao, S.S. (1997). Monkey cutaneous SAI and RA responses to raised and depressed scanned patterns: effects of width, height, orientation, and a raised surround. J. Neurophysiol. *78*, 2503–2517.

Boundy-Singer, Z.M., Saal, H.P., and Bensmaia, S.J. (2017). Speed Invariance of Tactile Texture Perception. J. Neurophysiol. *118*, jn.00161.2017.

Bourgeon, S., Dépeault, A., Meftah, E.-M., and Chapman, C.E. (2016). Tactile texture signals in primate primary somatosensory cortex and their relation to subjective roughness intensity. J. Neurophysiol. *115*, 1767–1785.

Burton, H., and Sinclair, R.J. (1994). Representation of tactile roughness in thalamus and somatosensory cortex. Can. J. Physiol. Pharmacol. *72*, 546–557.

Cadieu, C.F., Hong, H., Yamins, D.L.K., Pinto, N., Ardila, D., Solomon, E.A., Majaj, N.J., and DiCarlo, J.J. (2014). Deep Neural Networks Rival the Representation of Primate IT Cortex for Core Visual Object Recognition. PLoS Comput. Biol. *10*.

Callier, T., Saal, H.P., Davis-Berg, E.C., and Bensmaia, S.J. (2015). Kinematics of unconstrained tactile texture exploration. J. Neurophysiol. jn.00703.2014.

Chapman, C.E., Tremblay, F., Jiang, W., Belingard, L., and Meftah, E.M. (2002). Central neural mechanisms contributing to the perception of tactile roughness. In Behavioural Brain Research, pp. 225–233.

Connor, C.E., and Johnson, K.O. (1992). Neural coding of tactile texture: comparison of spatial and temporal mechanisms for roughness perception. J. Neurosci. *12*, 3414–3426.

Connor, C.E., Hsiao, S.S., Phillips, J.R., and Johnson, K.O. (1990). Tactile roughness: neural codes that account for psychophysical magnitude estimates. J. Neurosci. *10*, 3823–3836.

Croner, L.J., and Kaplan, E. (1995). Receptive fields of P and M ganglion cells across the primate retina. Vision Res. *35*, 7–24.

Darian-Smith, I., and Kenins, P. (1980). Innervation density of mechanoreceptive fibres supplying glabrous skin of the monkey's index finger. J. Physiol. *309*, 147–155.

Delhaye, B.P., Lieber, J.D., Mclellan, K.R., and Bensmaia, S.J. (2019). Feeling fooled: Texture contaminates the neural code for tactile speed.

Dépeault, A., Meftah, E.-M., and Chapman, C.E. (2013). Neuronal correlates of tactile speed in primary

somatosensory cortex. J. Neurophysiol. *110*, 1554–1566.

DiCarlo, J.J., and Cox, D.D. (2007). Untangling invariant object recognition. Trends Cogn. Sci. *11*, 333–341.

DiCarlo, J.J., and Johnson, K.O. (1999). Velocity invariance of receptive field structure in somatosensory cortical area 3b of the alert monkey. J. Neurosci. *19*, 401–419.

DiCarlo, J.J., and Johnson, K.O. (2000). Spatial and temporal structure of receptive fields in primate somatosensory area 3b: effects of stimulus scanning direction and orientation. J. Neurosci. *20*, 495–510.

Elsayed, G.F., Lara, A.H., Kaufman, M.T., Churchland, M.M., and Cunningham, J.P. (2016). Reorganization between preparatory and movement population responses in motor cortex. Nat. Commun.

Enroth-Cugell, C., and Robson, J.G. (1966). The contrast sensitivity of retinal ganglion cells of the cat. J. Physiol. *187*, 517–552.

Essick, G.K., and Edin, B.B. (1995). Receptor encoding of moving tactile stimuli in humans. II. The mean response of individual low-threshold mechanoreceptors to motion across the receptive field. J. Neurosci.

Finn, I.M., Priebe, N.J., and Ferster, D. (2007). The Emergence of Contrast-Invariant Orientation Tuning in Simple Cells of Cat Visual Cortex. Neuron *54*, 137–152.

Gallego, J.A., Perich, M.G., Naufel, S.N., Ethier, C., Solla, S.A., and Miller, L.E. (2018). Cortical population activity within a preserved neural manifold underlies multiple motor behaviors. Nat. Commun.

Gamzu, E., and Ahissar, E. (2001). Importance of temporal cues for tactile spatial- frequency discrimination. J Neurosci *21*, 7416–7427.

Goodwin, A.W., and Morley, J.W. (1987a). Sinusoidal Movement of a Grating Across the Monkey's Fingerpad: Representation of Grating and Movement Features in Afferent Fiber Responses. J. Neurosci. *7*, 2168–2180.

Goodwin, A.W., and Morley, J.W. (1987b). Sinusoidal movement of a grating across the monkey's fingerpad: effect of contact angle and force of the grating on afferent fiber responses. J. Neurosci. *7*, 2192–2202.

Handel, S., and Erickson, M.L. (2001). A Rule of Thumb: The Bandwidth for Timbre Invariance Is One Octave. Music Percept. *19*, 121–126.

Van Hateren, J.H., and Ruderman, D.L. (1998). Independent component analysis of natural image sequences yields spatio-temporal filters similar to simple cells in primary visual cortex. Proc. R. Soc. B Biol. Sci.

Hong, H., Yamins, D.L.K., Majaj, N.J., and Dicarlo, J.J. (2016). Explicit information for category-orthogonal object properties increases along the ventral stream. Nat. Neurosci. *19*, 613–622.

Johansson, R., and Vallbo, Å. (1979). Tactile sensibility in the human hand: relative and absolute densities of four types of mechanoreceptive units in glabrous skin. J. Physiol. 283–300.

Johansson, R.S., Landstrom, U., and Lundstrom, R. (1982). Responses of Mechanoreceptive Afferent Units in the Glabrous Skin of the Human Hand to Sinusoidal Skin Displacements. Brain Res. *244*, 17–25.

Joris, P.X., Bergevin, C., Kalluri, R., Mc Laughlin, M., Michelet, P., van der Heijden, M., and Shera, C.A. (2011). Frequency selectivity in Old-World monkeys corroborates sharp cochlear tuning in humans. Proc.

Natl. Acad. Sci. *108*, 17516–17520.

Kobak, D., Brendel, W., Constantinidis, C., Feierstein, C.E., Kepecs, A., Mainen, Z.F., Qi, X.L., Romo, R., Uchida, N., and Machens, C.K. (2016). Demixed principal component analysis of neural population data. Elife.

LaMotte, R.H., and Mountcastle, V.B. (1975). Capacities of humans and monkeys to discriminate vibratory stimuli of different frequency and amplitude: a correlation between neural events and psychological measurements. J. Neurophysiol. *38*, 539–559.

Lederman, S.J. (1974). Tactile roughness of grooved surfaces: The touching process and effects of macro- and microsurface structure. Percept. Psychophys. *16*, 385–395.

Lederman, S.J. (1981). The perception of surface roughness by active and passive touch. Bull. Psychon. Soc. *18*, 253–255.

Lederman, S.J., and Taylor, M.M. (1972). Fingertip force, surface geometry, and the perception of roughness by active touch. Percept. Psychophys. *12*, 401–408.

Lewicki, M.S. (2002). Efficient coding of natural sounds. Nat. Neurosci.

Libouton, X., Barbier, O., Plaghki, L., and Thonnard, J.L. (2010). Tactile roughness discrimination threshold is unrelated to tactile spatial acuity. Behav. Brain Res. *208*, 473–478.

Lieber, J.D., and Bensmaia, S.J. (2019). High-dimensional representation of texture in somatosensory cortex of primates. Proc. Natl. Acad. Sci.

Lieber, J.D., Xia, X., Weber, A.I., and Bensmaia, S.J. (2017). The Neural Code for Tactile Roughness in the Somatosensory Nerves. J. Neurophysiol. jn.00374.2017.

Mackevicius, E.L., Best, M.D., Saal, H.P., and Bensmaia, S.J. (2012). Millisecond Precision Spike Timing Shapes Tactile Perception. J. Neurosci. *32*, 15309–15317.

Marozeau, J., de Cheveigné, A., McAdams, S., and Winsberg, S. (2003). The dependency of timbre on fundamental frequency. J. Acoust. Soc. Am. *114*, 2946.

Meftah el-M, Belingard, L., and Chapman, C.E. (2000). Relative effects of the spatial and temporal characteristics of scanned surfaces on human perception of tactile roughness using passive touch. Exp. Brain Res. *132*, 351–361.

Metzen, M.G., Hofmann, V., and Chacron, M.J. (2016). Neural correlations enable invariant coding and perception of natural stimuli in weakly electric fish. Elife *5*.

Morley, J.W., Goodwin, A.W., and Darian-Smith, I. (1983). Tactile discrimination of gratings. Exp. Brain Res. *49*, 291–299.

Olshausen, B.A., and Field, D.J. (1996). Emergence of simple-cell receptive field properties by learning a sparse code for natural images. Nature *381*, 607–609.

Olshausen, B.A., and Field, D.J. (2004). Sparse coding of sensory inputs. Curr. Opin. Neurobiol. *14*, 481–487.

Paré, M., Behets, C., and Cornu, O. (2003). Paucity of presumptive Ruffini corpuscles in the index finger pad of humans. J. Comp. Neurol. *456*, 260–266.

Phillips, J.R., Johansson, R.S., and Johnson, K.O. (1992). Responses of human mechanoreceptive afferents to embossed dot arrays scanned across fingerpad skin. J. Neurosci. *12*, 827–839.

Rust, N.C., and DiCarlo, J.J. (2010). Selectivity and Tolerance ("Invariance") Both Increase as Visual Information Propagates from Cortical Area V4 to IT. J. Neurosci. *30*, 12978–12995.

Saal, H.P., Harvey, M.A., and Bensmaia, S.J. (2015). Rate and timing of cortical responses driven by separate sensory channels. Elife *4*.

Saal, H.P., Suresh, A.K., Solorzano, L.E., Weber, A.I., and Bensmaia, S.J. (2017). The effect of contact force on the responses of tactile nerve fibers to scanned textures. Neuroscience.

Sachs, M.B., and Young, E.D. (1979). Encoding of steady-state vowels in the auditory nerve: Representation in terms of discharge rate. J. Acoust. Soc. Am. *66*, 470.

Sadagopan, S., and Wang, X. (2008). Level Invariant Representation of Sounds by Populations of Neurons in Primary Auditory Cortex. J. Neurosci. *28*, 3415–3426.

Sinclair, R.J., and Burton, H. (1991). Neuronal activity in the primary somatosensory cortex in monkeys (Macaca mulatta) during active touch of textured surface gratings: responses to groove width, applied force, and velocity of motion. J. Neurophysiol. *66*, 153–169.

Sripati, A.P., Yoshioka, T., Denchev, P., Hsiao, S.S., and Johnson, K.O. (2006). Spatiotemporal receptive fields of peripheral afferents and cortical area 3b and 1 neurons in the primate somatosensory system. J. Neurosci. *26*, 2101–2114.

Talbot, W.H., Darian-Smith, I., Kornhuber, H.H., and Mountcastle, V.B. (1968). The Sense of Flutter Vibration Comparison of the Human Capacity With Response Patterns of Mechanoreceptive Afferents From the Monkey Hand. J. Neurophysiol. *31*, 301.

Tanaka, Y., Bergmann Tiest, W.M., Kappers, A.M.L., and Sano, A. (2014). Contact force and scanning velocity during active roughness perception. PLoS One *9*.

Town, S.M., Wood, K.C., and Bizley, J.K. (2018). Sound identity is represented robustly in auditory cortex during perceptual constancy. Nat. Commun.

Tremblay, F., Ageranioti-Bélanger, S. a, and Chapman, C.E. (1996). Cortical mechanisms underlying tactile discrimination in the monkey. I. Role of primary somatosensory cortex in passive texture discrimination. J. Neurophysiol. *76*.

Walker, K.M.M., Bizley, J.K., King, A.J., and Schnupp, J.W.H. (2011). Multiplexed and Robust Representations of Sound Features in Auditory Cortex. J. Neurosci. *31*, 14565–14576.

Weber, A.I., Saal, H.P., Lieber, J.D., Cheng, J.-W., Manfredi, L.R., Dammann, J.F., and Bensmaia, S.J. (2013). Spatial and temporal codes mediate the tactile perception of natural textures. Proc. Natl. Acad. Sci. U. S. A. *110*, 17107–17112.